



# Energy absorption behavior of tapered and ribbed thin-walled structures under compressive crushing forces

Mehmet Seha Tatlier\*

Mechanical Engineering, Osmaniye Korkut Ata University, 80000 Osmaniye, Turkey

Received: 30 January 2021; Accepted: 25 August 2021

This paper investigates the energy absorption behavior of straight and tapered square, hexagonal and octagonal tubes with two types ribbed connection inside. The parameters studied are the geometry of section, rib configuration and taper angle. In this study, a numerical model is introduced and justified by both the analytical and numerical models in the literature. The results show that octagonal tubes have the highest energy absorption capacity followed by hexagonal and square sections. The ribbed profiles have better energy absorption per unit mass by an increased number of corners. The energy absorption per unit mass and crushing force efficiency decrease with increasing taper angle. Results also indicate that the tapered profile delivers more stable crushing behavior. The research findings can be used to quantify energy absorption in the design of energy absorbers for impact applications.

**Keywords:** Auxetic, Energy absorption, Crush, Dynamic crushing strength, Impact

## 1 Introduction

The advances in technology allow designers seek new designs to absorb energy in transportation vehicles. The researchers have paid a significant focus on the use of impact energy absorbers to avoid loss of life and damage. The energy absorbers are mainly designed from thin-walled structures due to their low weight, low cost, and ease of production. The energy absorbers dissipate energy by converting kinetic energy into plastic deformation energy. The energy absorbers are designed with triangular, circular, square, and other polygonal cross-sections and can be employed by metallic and polymeric foams to increase their effectiveness.

The quantitative measure of the absorbed energy can be obtained by means of mechanics as well as the mean crushing forces. Axial loading of cylinders is first introduced by Alexander<sup>1</sup> as energy absorbers in the 60s by identifying the folding mechanism of thin-walled structures. Later, Wierzbicki and Abramowicz and<sup>2,3</sup>, Abramowicz and Jones<sup>4,5</sup> and Andrews *et al.*<sup>6</sup> conducted experimental and theoretical research to investigate the circular and square tubes under quasi-static and dynamic loading conditions. Wierzbicki and Abramowicz and<sup>2,3</sup> introduced a super folding element (SFE) theory based on analysis of the hinges

at the folds and is used to predict the mean crushing load of polygonal sections. This theory later was modified to fit experimental results<sup>2</sup>.

Langseth and Hopperstad<sup>7</sup> performed experiments of aluminum square cross-sectional thin-wall structures on a comparison of the quasi-static and dynamic loadings. In their study, they showed quasi-static mean crushing forces are higher than dynamic mean crushing forces. Moreover, they showed folding mechanisms of circular and square cross-sections are similar to a peak crushing force at the beginning of the crush while it oscillates through the crushing. Thin-walled structures with triangular, circular, square cross-sections with tapered profiles are studied employing numerical and experimental works by Alavi Nia and Hamedani<sup>8</sup>.

Mamalis *et al.*<sup>9</sup> studied the crumpling mechanism of thin-walled octagonal steel tubes that were subjected to axial static and dynamic compression. They found out that octagonal structures absorb more energy compared to the square structure while there is little discrepancy between circular cross-sections. Zhang and Zhang<sup>10</sup> investigate the energy absorption characteristics of polygonal and rhombic columns under quasi-static loading in addition to numerical investigation of the polygonal and angle element columns under quasi-static and dynamic axial compression.

\*Corresponding author (E-mail: sehatatlier@osmaniye.edu.tr)

Multi-cell cross-sections have been grabbed significant interest in recent years due to their high energy absorption to weight ratio. Chen and Wierzbicki<sup>11</sup> developed a theoretical model to address the crushing of thin-walled structures with multicell sections and confirmed their results with numerical solutions. Kim<sup>12</sup> studied new geometries of the cross-section for energy absorber structures and compared new designs with conventional square cross-sections. His analytical model predicts the mean crushing forces in new multi-cell profiles efficiently and results agree well with the numerical model. According to his study specific absorbed energy (SEA) increases up to 90% adding extra profiles to the conventional square cross-sections.

Alavi Nia and Parsapour<sup>13</sup> revised the analytical derivation developed by Zhang<sup>14</sup> to predict the mean crushing force for unequal sized cells and then analytical and numerical results are validated with experiments. Zhang and Zhang<sup>15</sup> investigated the energy absorption characteristics of angle elements with three panels and proposed a theoretical model to estimate the crush resistance of the three-panel angle elements. Hou et. al<sup>16</sup> aimed to design the multi-cell cross-sectional thin-walled columns by maximizing energy absorption and minimizing the peak crush force. Najafi and Rais-Rohani<sup>17</sup> performed finite element simulations to study the energy absorption characteristics of axially crushed thin-walled aluminum tubes with different multi-cell, multi-corner configurations. Moreover, they derived an analytical model to predict the mean crushing force which delivered good agreement with the numerical solution. Zhang and Zhang<sup>18</sup> conducted a study to investigate the connected cellular structures by modeling represented element volume. They developed an analytical model which was justified by experiment to investigate the different angle and connectivity configurations. Tang *et al.*<sup>19</sup> performed numerical studies and they were able to show that circular profiles absorb more energy than equivalent square profiles.

## 2 Materials and Methods

The numerical simulations for the axial crushing of tubes are performed in ABAQUS Explicit. The

impactors are modeled with rigid shell elements with an impact mass of 90 kg. The quadrilateral finite-membrane-strain element S4R with a thickness of 1.5 mm is utilized as shell elements in the finite element analyses. Five integration points are employed through the shell thickness to model bending. The material used in this work is a typical mild steel with a yield strength of 304 MPa and hardening characteristics were obtained by standard tensile tests. The true stress and strain data from Nagel and Thambiratnam<sup>20</sup> are utilized for the numerical solution and presented in Table 1.

The element size 5 mm inputted to FE solver after ensuring the convergence. The impact side of tubes is set free while other ends of tubes constrained to the rigid bottom surface which is fixed. The impactors strike the tubes from their smaller end in tapered tubes. The length of the tubes is 300 mm and the cross-sections are 100 mm x 100mm while dimensions of other cross-sections are given in Fig. 1. The strain effect is addressed by employing Copwer-Symonds model expressed in Eq. 1 to analyze the crushing of tubes.

$$\dot{\epsilon}_p = D \left( \frac{\sigma_0'}{\sigma_0} - 1 \right)^q \text{ for } \sigma_0' \geq \sigma_0 \quad \dots (1)$$

$\sigma_0'$  is the dynamic flow stress at a uniaxial plastic strain rate  $\dot{\epsilon}_p$  and  $\sigma_0$  is the associated static flow stress. the material parameters  $D = 6844 \text{ s}^{-1}$  and  $q = 3.91$  were utilized in previous studies<sup>4,5,20,21</sup> and they are implemented in the presented finite element model as the overstress power law. The automatic contact algorithm is adapted because of the complexity of deformation.

### 2.1. Validation

The finite element model for dynamic loading is justified with the theoretical and numerical models previously published a study of Nagel and Thambiratnam<sup>22</sup>. In the validation models, wall thickness  $h = 1.5 \text{ mm}$ , taper angle  $\theta = 10^\circ$ ,  $v$  impact velocity,  $m = 90 \text{ kg}$  impact mass and with a length of 300 mm shown in Fig. 1(a). In dynamic crushing force is obtained from presented finite element model

Table 1 — True stress-plastic data points used for mild steel in FEM<sup>20</sup>

$\sigma_t$ (MPa)	304.6	344.19	385.15	424.88	450.39	470.28
$\epsilon_p$	0	0.0244	0.0485	0.0951	0.1384	0.1910

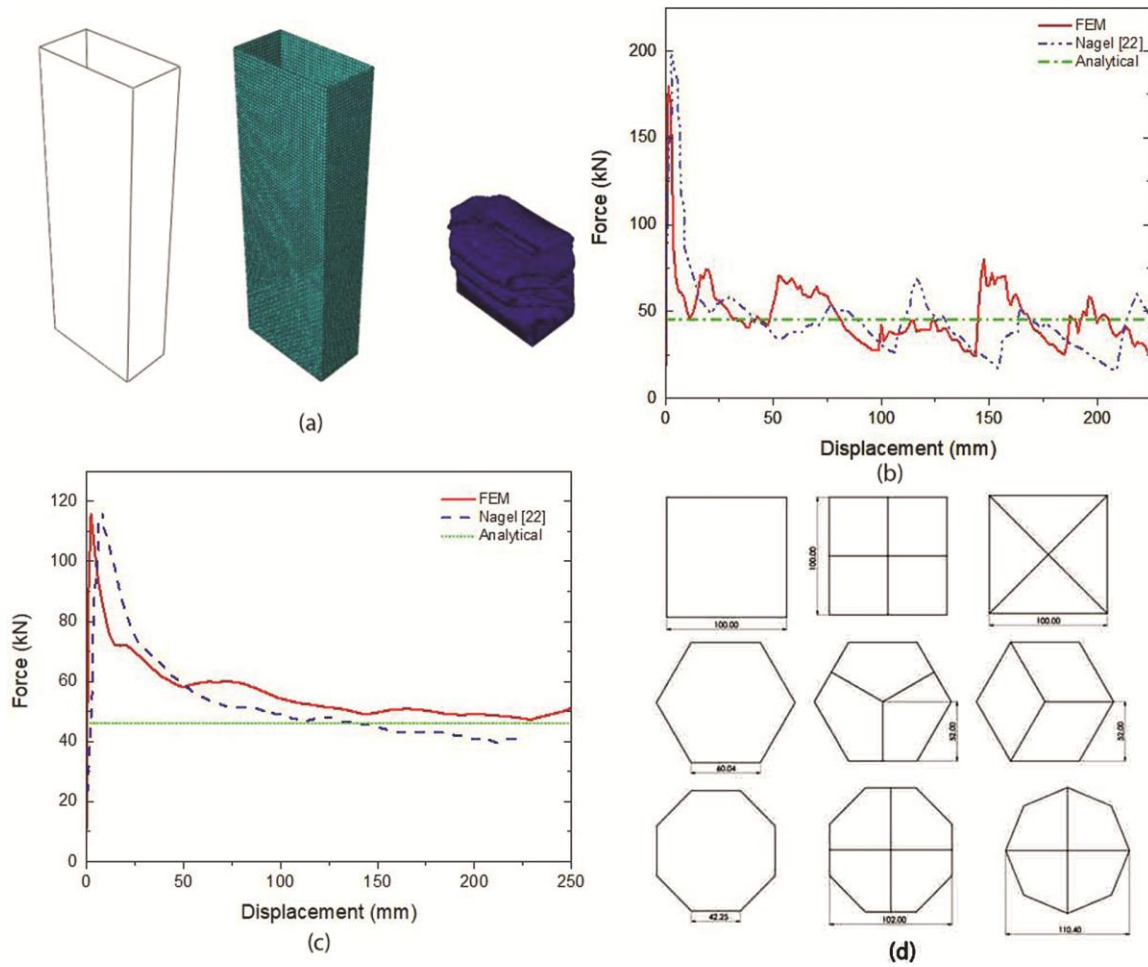


Fig. 1 (a) — Rectangular tube used for validation, (b) Dynamic force displacement graph of rectangular tube 50mm x 100mm (c) Mean dynamic crushing force of straight rectangular tube of 50mm x 100mm dimension, and (d) Sections and dimensions of tubes: first column no ribs, the second column is Type-I, and third column Type-II ribs

is compared with numerical and analytical model discussed in Nagel and Thambiratnam<sup>22</sup>. The present finite element model well agrees with both numerical and analytical models. Also, the mean crushing force delivered by the presented finite element model is compared with the numerical and analytical model discussed in Nagel and Thambiratnam<sup>22</sup> too. Results not only in Fig. 1(b) but also Fig. 1(c) illustrates the effectiveness of the presented finite element model. Hereafter proposed finite element model is utilized to study the energy absorption characteristics of straight and tapered tubes with inside rip reinforcements.

**2.2. Analysis**

In this study several straight tubes with different cross-sections and rip configuration. The tubes studied in this work are tapered by 5°, 7.5°, and 10°. For each square, hexagonal, and octagonal section three types of models are developed. The first model

Table 2 — Model codes

Geometry	Code	Rib Style	Code	Tapering	Code
Square	Sq	No ribs	R0	5°	T5
Hexagon	Hx	Type-I	R1	7.5°	T7.5
Octagon	Oc	Type-II	R2	10°	T10

is free of ribs, the second model consists of ribs connecting from the middle of the sides to the center, and ribs are connected from the corner of the cross-section to the middle in the third model. The model codes are introduced for clarity in Table 2.

The absorbed energy is calculated from the area under the load-displacement curves by Eq. (2). Meanwhile, the mean crushing force can be calculated from total absorbed energy and total displacement as in Eq. (3). Crush force efficiency (CFE) is a useful measure for the uniformity of the collapse force. CFE is defined as the ratio of the mean crushing force to the peak crushing force as in Eq. (4). CFE must be

100% for an ideal energy absorber. The specific energy absorption (SEA) is an important parameter for devices that require high energy absorption to weight ratio. SEA is the energy absorbed by the unit mass which is calculated by Eq. (5) hence its unit is kj/kg.

$$EA = \int_0^\delta F d\delta \quad \dots (2)$$

$$F_m = \frac{EA}{\delta} \quad \dots (3)$$

$$CFE = \frac{F_m}{F_{max}} \quad \dots (4)$$

$$SEA = \frac{EA}{m} \quad \dots (5)$$

**3 Results and Discussion**

In this study, the tubes in Fig. 1(d) with different cross-sections, rip configurations and tapering angles are studied for their energy absorbance capacity and crushing deformation mechanism. The tubes studied

in this work are tapered by 5°, 7.5°, and 10° as seen in Fig. 2(a). The force-displacement curves are obtained from the numerical analysis for the calculation of the energy absorbed during the crush as well as the peak load.

The tube masses are arranged to be close to each other however they still have different masses. Hence it is more objective to compare the SEA specific absorbed energy of the tubes. The SEA values are compared with each other and it is obvious that ripped tubes dissipate more energy than those without ribs. In thin-walled structures, most energy dissipation is governed by the formation of plastic hinges during the crushing of the tubes. The increase in the energy dissipation of ripped structures could be attributed to the higher number of the formation of the plastic hinge. According to the results, the energy absorption increases with the increase of the number of sides. Figure 2(b-d) show the force-displacement graph of the square, hexagonal, and octagonal tubes without ribs. According to Fig. 2(b-d) as the sides of the polygons increase energy dissipation per unit mass also increases. There is a significant increase in the energy absorption of tubes with the implementation of ribs as presented in Fig. 3(a-c). Type-I ribs cause better energy absorption than Type-II ribs which is

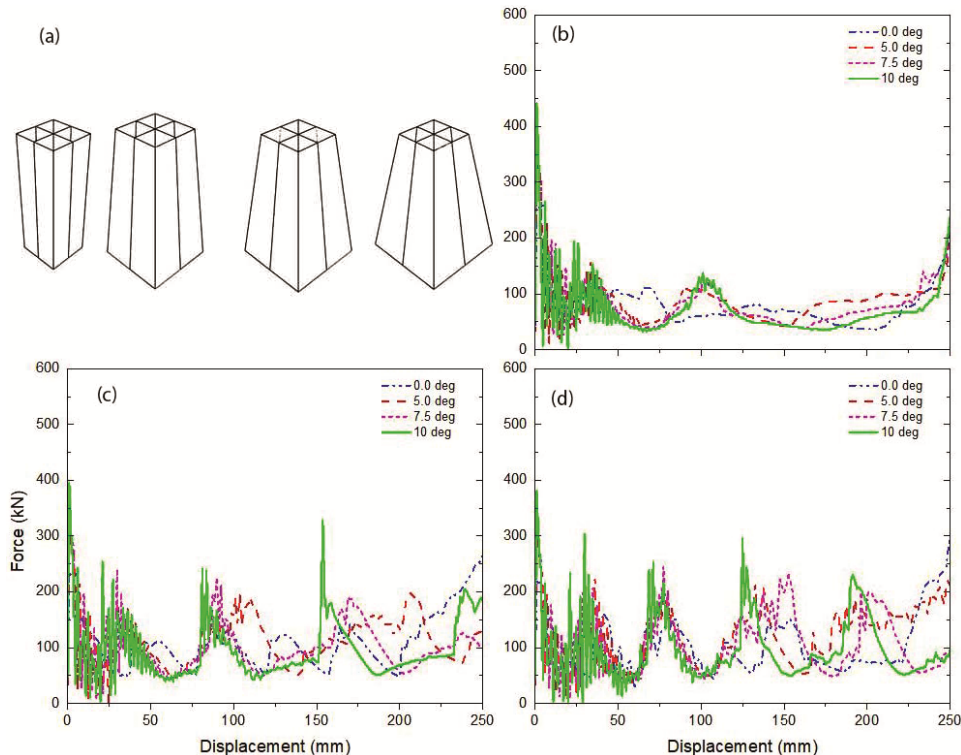


Fig. 2 (a) — Tapering of square tubes with Type I ribs by angles of 0°, 5°, 7.5°, and 10°, respectively, (b) Square tubes with no ribs, (c) Hexagonal tube without ribs, and (d) Octagonal tube without ribs.

better energy absorber than tubes without ribs as seen in Fig. 3(d), and Fig. 4(a and b). The Type-I and without ribs dissipate the most and the least energy, respectively as observed in Fig. 4(c and d), and

Fig. 5(a). This result is interpreted that the energy absorbed by the tubes increases with the increase of the number of junctions. For instance, squares with Type-I ribs have eight conjunctions while simple and

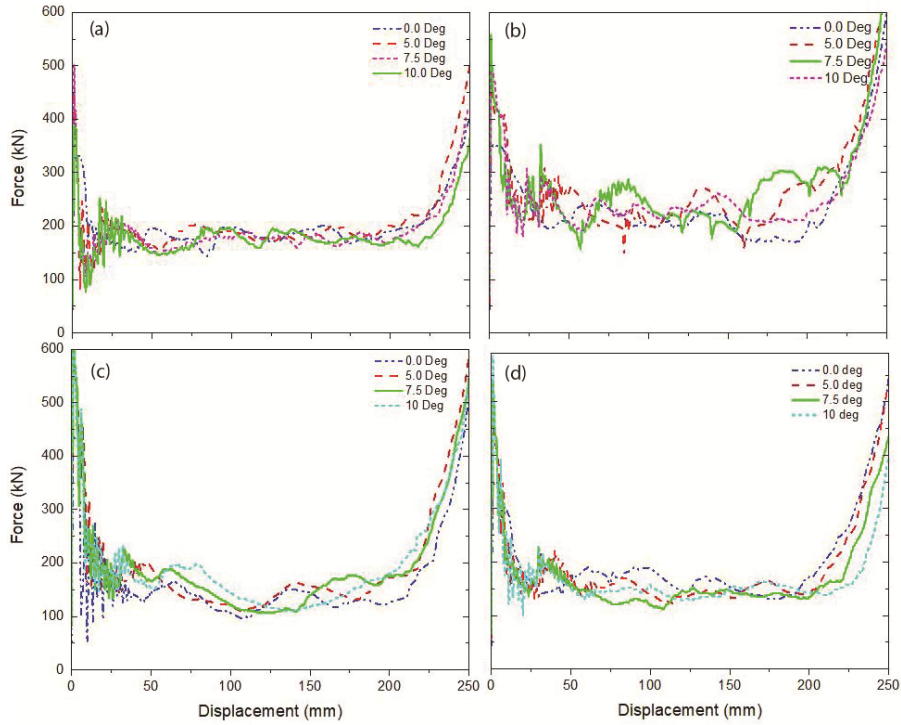


Fig. 3(a) — Square tubes with Type I ribs, (b) Hexagonal tubes with Type I ribs, (c) Octagonal tubes with Type I ribs, and (d) Square tubes with Type II ribs.

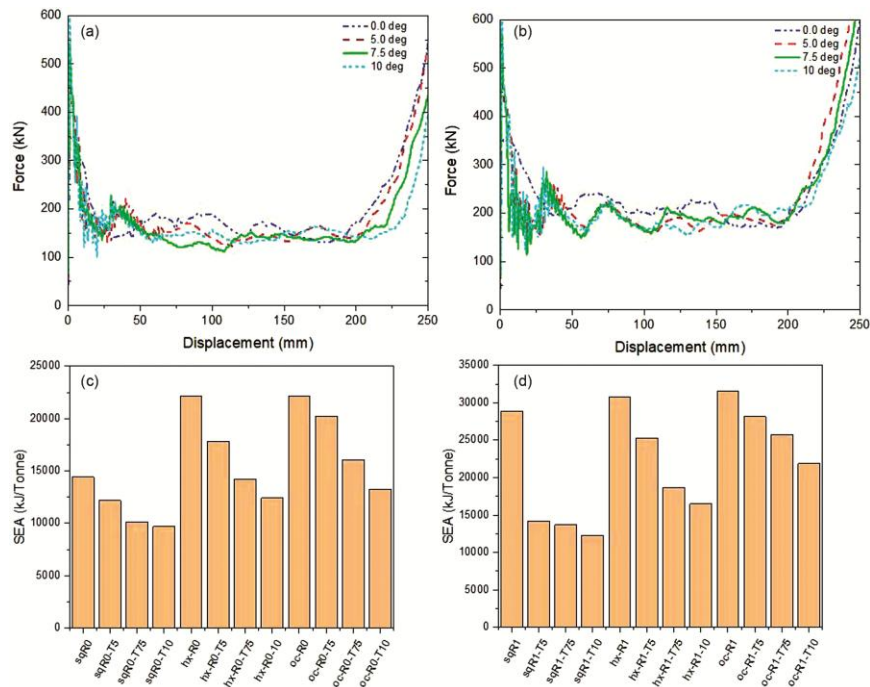


Fig. 4 — (a)-2 Hexagonal tubes with type II ribs, (b) Octagonal tubes with Type II ribs, (c) SEA values of tubes without ribs, and (d) SEA values of tubes with Type-I ribs.

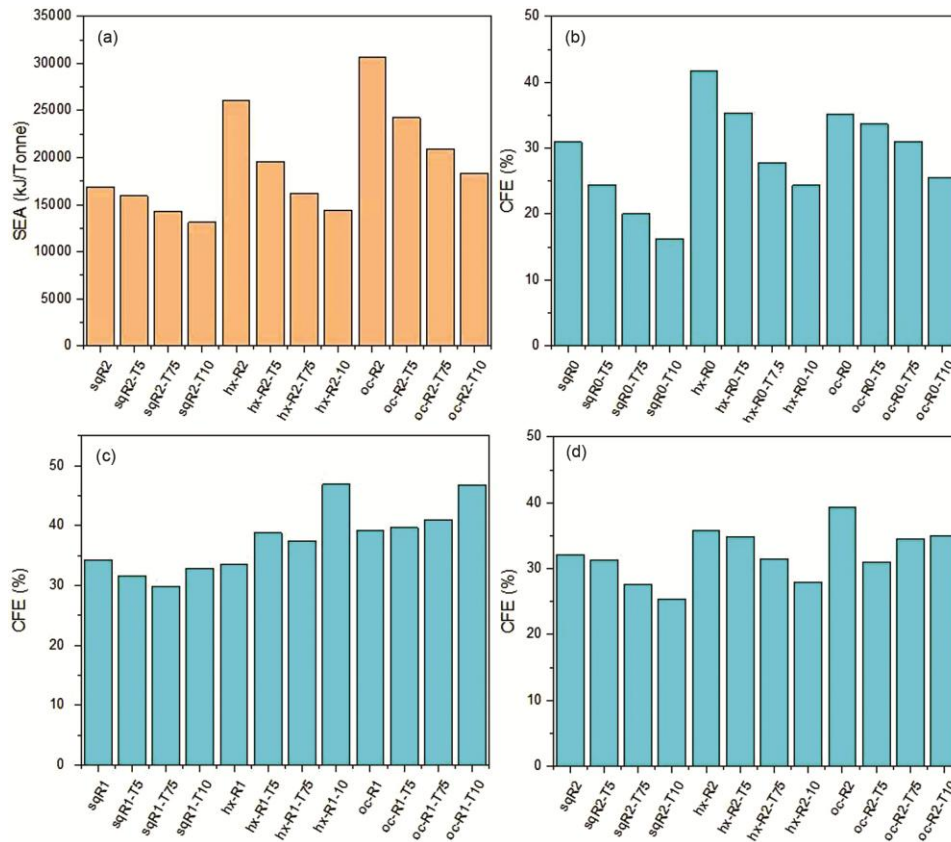


Fig. 5 — (a) SEA values of tubes with Type-II ribs, (b) CFE values of tubes without ribs, (c) CFE values of tubes with Type-I ribs, and (d) CFE values of tubes with Type-II ribs.

Type-II ripped tubes have four junctions. The junctions require more energy for plastic bending formation hence enhancing the energy absorption properties of the tubes.

CFE values of different sections also differ with the rib type and tapering angle. In Fig. 5(b), the sections do not have any ribs. Although CFE values increase from square to octagonal sections, it decreases as the tapering angle increases. On the other hand, in Fig. 5(c), CFE increases with an increasing number of sides, while there is no significant change in the tapering angle of sections with Type-I rib connections. According to Fig. 5(d), sections with Type-II rib configuration exhibit an insignificant increase in CFE by the change of sections. Similarly, CFE values slightly decrease with increasing taper angle. According to the findings of this research, larger taper angles neither increase SEA nor CFE for a given section under the conditions discussed.

#### 4 Conclusion

In this work, mechanical behaviors of thin-walled mild steel structures with square, hexagonal, and octagonal sections including ribs and tapering angles

under dynamic compression were studied. The simulations were done by ABAQUS software and compared with the previous analytical and numerical models in published works. The model presented in this study delivered good agreement with previous numerical and analytical models hence further study conducted after the verification of the numerical model. A comparison of the results showed that ribbed sections had greater SEA than the structures without ribs. Besides, tubes with ribs exhibit enhanced CFE values. SEA increases as the number of sides of the section increase. Octagonal sections absorb more energy than hexagonal while hexagonal sections absorb more than square sections. The results of this investigation show that the tapering of the tubes decreases the SEA and CFE of tubes. However, the peak loads tend to decrease with the increase of the tapering angle. Moreover, dynamic crushing forces fluctuation smooths better for high tapering angles.

#### References

- 1 Alexander J M Q, *J Mech Appl Math*, 13 (1960) 10.
- 2 Wierzbicki T, & Abramowicz W, *J Appl Mech Trans ASME*, 50 (1983) 727.

- 3 Abramowicz W, & Wierzbicki T, *J Appl Mech*, 56 (1989) 113.
- 4 Abramowicz W, & Jones N, *Int J Impact Eng*, 2 (1984) 179.
- 5 Abramowicz W, & Jones N, *Int J Impact Eng*, 4 (1986) 243.
- 6 Andrews K R F, England G L, & Ghani E, *Int J Mech Sci*, 25 (1983) 687.
- 7 Langseth M, & Hopperstad O S, *Int J Impact Eng*, 18 (1996) 949.
- 8 Alavi Nia A, & Parsapour M, *Thin-Walled Struct*, 74 (2014) 155.
- 9 Mamalis A G, Manolakos D E, Baldoukas A K, & Viegelaan G L, *Thin-Walled Struct*, 12 (1991) 17.
- 10 Zhang X, & Zhang H, *Thin-Walled Struct*, 57 (2012) 25.
- 11 Chen W, & Wierzbicki T, *Thin-Walled Struct*, 39 (2001) 287.
- 12 Kim H S, *Thin-Walled Struct*, 40 (2002) 311.
- 13 Alavi Nia A, & Parsapour M, *Thin-Walled Struct*, 68 (2013) 26.
- 14 Zhang X, Cheng G, & Zhang H, *Thin-Walled Struct*, 44 (2006) 1185.
- 15 Zhang X, & Zhang H, *Int J Impact Eng* 46 (2012) 23.
- 16 Hou S, Li Q, Long S, Yang X, & Li W, *Int J Impact Eng*, 35 (2008) 1355.
- 17 Najafi A, & Rais-Rohani M, *Thin-Walled Struct*, 49 (2011) 1.
- 18 Zhang X, & Zhang H, *Int J Impact Eng*, 57 (2013) 81.
- 19 Tang, Z, Liu S, & Zhang Z, *Thin-Walled Struct*, 62 (2013) 75.
- 20 Nagel G M, & Thambiratnam D P, *Int J Impact Eng*, 32 (2006) 1595.
- 21 Reid S R, Reddy T Y, & Gray M D, *Int J Mech Sci*, 28 (1986) 295.
- 22 Nagel G M, & Thambiratnam D P, *Int J Crashworthiness*, 9 (2004) 389.